AGU PUBLICATIONS

Water Resources Research

RESEARCH ARTICLE
10.1002/2016WR020187

Key Points:
- Tropical mountain catchments with perennially humid climates still have varying interannual source contributions
- The riparian zone is the most important source contributor, and younger stream water in wet conditions is affected by water from hillslopes
- EMMA, hydrograph separation and ITTPs based on multitracer sets are used to understand hydrological processes in headwater catchments

Supporting Information:
- Supporting Information S1
- Table S1

Correspondence to:
A. Correa,
Alicia.Correa@umwelt.uni-giessen.de

Citation:
Correa, A., D. Windhorst, D. Tetzlaff, P. Crespo, R. Célleri, J. Feyen, and L. Breuer (2017), Temporal dynamics in dominant runoff sources and flow paths in the Andean Páramo, *Water Resour. Res.*, *53*, 5998–6017, doi:10.1002/2016WR020187.

Received 25 NOV 2016
Accepted 27 JUN 2017
Accepted article online 5 JUL 2017
Published online 24 JUL 2017

Temporal dynamics in dominant runoff sources and flow paths in the Andean Páramo

Alicia Correa[1,2], David Windhorst[2], Doerthe Tetzlaff[3], Patricio Crespo[1], Rolando Célleri[1], Jan Feyen[1], and Lutz Breuer[2,4]

[1]Departamento de Recursos Hídricos y Ciencias Ambientales, Facultad de Ciencias Agropecuarias, Facultad de Ingeniería, Universidad de Cuenca, Cuenca, Ecuador, [2]Institute for Landscape Ecology and Resources Management, Justus Liebig University Giessen, Giessen, Germany, [3]Northern Rivers Institute, School of Geoscience, University of Aberdeen, Aberdeen, Scotland, UK, [4]Centre for International Development and Environmental Research, Justus Liebig University Giessen, Giessen, Germany

Abstract The relative importance of catchment's water provenance and flow paths varies in space and time, complicating the conceptualization of the rainfall-runoff responses. We assessed the temporal dynamics in source areas, flow paths, and age by End Member Mixing Analysis (EMMA), hydrograph separation, and Inverse Transit Time Proxies (ITTPs) estimation within a headwater catchment in the Ecuadorian Andes. Twenty-two solutes, stable isotopes, pH, and electrical conductivity from a stream and 12 potential sources were analyzed. Four end-members were required to satisfactorily represent the hydrological system, i.e., rainfall, spring water, and water from the bottom layers of Histosols and Andosols. Water from Histosols in and near the riparian zone was the highest source contributor to runoff throughout the year (39% for the drier season, 45% for the wetter season), highlighting the importance of the water that is stored in the riparian zone. Spring water contributions to streamflow tripled during the drier season, as evidenced by geochemical signatures that are consistent with deeper flow paths rather than shallow interflow through Andosols. Rainfall exhibited low seasonal variation in this contribution. Hydrograph separation revealed that 94% and 84% is preevent water in the drier and wetter seasons, respectively. From low-flow to high-flow conditions, all the sources increased their contribution except spring water. The relative age of stream water decreased during wetter periods, when the contributing area of the riparian zone expands. The multimethod and multitracer approach enabled to closely study the interchanging importance of flow processes and water source dynamics from an interannual perspective.

1. Introduction

Knowledge of processes that control the rainfall-runoff behavior of high-elevation tropical mountain catchments is relevant because of the range of ecosystem services that these areas provide [*Buytaert et al*., 2006], especially in the Andean region, where surrounding communities mainly depend on the fresh water that is supplied by these ecosystems [*Buytaert et al*., 2006*; Célleri and Feyen*, 2009; *Roa-García et al*., 2011]. Regardless, the hydrologic functioning of the Andean Paramo (high-elevation Andean grassland) is only recently investigated remaining poorly understood. Recent evidence revealed that changes in land use and land cover are major drivers of hydrological alteration in the tropical Andes [*Ochoa-Tocachi et al*., 2016], and wetlands greatly affect the generation of moderate and high flows, which directly affects the water yield [*Mosquera et al*., 2015]. In previous research, *Correa et al*. [2016] noted that soils are the most relevant physiographic descriptor of the hydrological response and that the rainfall-runoff response is mainly controlled by a variable source area in the riparian zone. Another study showed that the stream water quality exhibits the greatest similarity to the water that is stored in the topsoil from the valley bottom and describes flow paths through the slopes and riparian area [*Mosquera et al*., 2016a]. However, far too little attention has been paid to improving our understanding through an interannual approach.

Flow paths vary on temporal and spatial scales; so unraveling the dynamics of hydrological-hydrochemical responses is rather complex [*Brown et al*., 1999; *Soulsby et al*., 2006; *Capell et al*., 2012]. Research in tracer hydrology has produced several applications to grasp this complexity, improve our understanding of the hydrological responses, and study, for example, the estimation of the main geographical runoff contributing sources [*Hooper*, 2003; *Liu et al*., 2004] and the tracking of flow paths [*McDonnell*, 2003; *Klaus and McDonnell*,

2013]. In this context, hydrochemical tracers are mostly used to identify the geographical runoff sources and their contribution by End Member Mixing Analysis (EMMA). In the EMMA approach, stream water is assumed to be an integrated mixture of different water sources, namely, end-members [*Christophersen et al*., 1990]. Generally, precipitation, throughfall, litter leachate, shallow and deep groundwater and soil water from hillslopes and riparian zones are considered key geographical end-members [*Inamdar et al*., 2013].

Stable water isotopes are commonly used to evaluate the temporal dynamics of flow paths and the relative importance of preevent and event water contributions [*Buttle*, 1994; *Klaus and McDonnell*, 2013]. Water-age distributions are frequently evaluated by mean transit time (MTT) calculations based on lumped parameter models and adjusted transit time distributions [*McGuire and McDonnell*, 2006], assuming that the resulting travel times reflect the mean over the entire period under consideration. Recent work proved that the MTT frequently exhibits aggregation errors [*Kirchner*, 2016a] and implicitly presumes stationarity. This assumption is often violated because every catchment in the real world exhibits nonstationarity and heterogeneous behavior in some degree [*McGuire and McDonnell*, 2006; *Kirchner*, 2016a, 2016b]. Interannual fluctuations and conditions outside the assumed stationary zones (e.g., during discharge events) are not considered by the MTT.

Kirchner [2016a, 2016b] introduced the concept of the fraction of young water (FYW) in streams as a metric of transit times, which is less sensitive to the spatial heterogeneity and nonstationarity compared to MTTs. FYW defines the fraction of water in the stream that is younger than a predefined age. For instance, *Jasechko et al*. [2016] recently used this metric to quantify the annual percentages of the FYW for several catchments around the globe. However, similar to the MTT, the FYW still requires relatively long data sets ($>$1 year) and does not allow an assessment of the interannual variability.

Our analysis of relative water ages is based on Inverse Transit Time Proxies (ITTPs) [*Tetzlaff et al.*, 2009] to overcome the limitations of MTTs and the FYW. Similar to the FYW and MTTs, ITTPs assess the temporal delay between an input signal (commonly rainfall) and the outgoing signal (commonly stream water). In contrast to the MTT, the temporal delay is reported as a dampening factor of the isotope signatures of those signals rather than an actual time. The simplicity of this approach enables to calculate ITTPs on a much shorter timespan than what is required for the FYW or MTT. ITTPs are therefore an alternative measure to represent the relative water ages and assess the interannual variability of water ages [*Tetzlaff et al*., 2009; *Seeger and Weiler*, 2014].

Generally, all these methods provide insight into the system from different perspectives and should ideally complement each other to depict the same hydrological processes; however, such methods are rarely combined with each other. This study combines several methods to elucidate the hydrological behavior of a Páramo covered catchment and analyze the temporal shift in the timing/response and the spatial shift in flow paths and source regions for different seasons and flow conditions. Several methods can support or contradict each other, thereby strengthening the interpretation and improving our understanding or revealing flaws in the selected methods.

The methods in this research include (1) geographical runoff source identification by End Member Mixing Analysis (EMMA) as part of the spatial domain [*Christophersen and Hooper*, 1992; *Hooper*, 2003]; (2) two-component hydrograph separation by stable water isotopes [*Klaus and McDonnell*, 2013]; and (3) the estimation of water ages by a simple measure of isotope signature damping with Inverse Transit Time Proxies (ITTPs) [*Tetzlaff et al*., 2009]. Furthermore, MTT estimations that were derived by *Mosquera et al*. [2016b] for the same study area are used to test the applicability of the ITTPs.

Data that were collected from 2012 to 2014 in the high tropical mountain Zhurucay Ecohydrological Observatory, which is situated in South Ecuador, are used to reach the following specific objectives: (1) to characterize our study area from hydroclimatic, hydrochemical, and isotopic perspective; (2) identify the dominant water sources of runoff generation; and (3) assess the temporal response of the water sources, the dynamics of the flow paths and the water ages.

2. Study Site

The study was conducted in the Zhurucay Ecohydrological Observatory, a small tropical headwater catchment (7.53 km^2) in South Ecuador, situated in the perennially humid Páramo region [*Josse et al*., 2009;

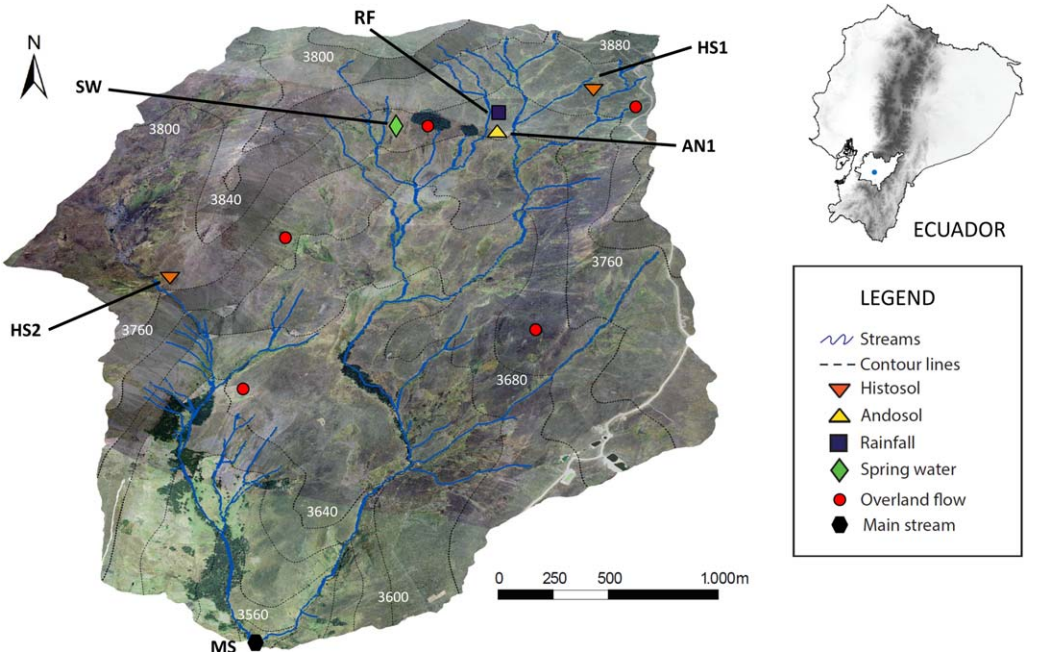

Figure 1. The Zhurucay River Ecohydrological Observatory (3D) located in southern Ecuador, showing the sites of water sampling: HS1 and HS2 represent the Histosol soil sampling sites; AN1 stands for the Andosol soil sampling site; RF represents rainfall measuring sites; SW stands for spring water, OF the overland flow, and MS are the main stream monitoring sites. White numbers represent meters above the sea level.

Ochoa-Tocachi et al., 2016]. The elevation within the catchment varies between 3505 and 3900 m asl (Figure 1). The annual rainfall averages 1345 mm [*Padrón et al.*, 2015], and the annual reference evapotranspiration is 723 mm as estimated by *Córdova et al.* [2015].

The average annual discharge is 864 mm yr^{-1} with an average runoff coefficient (RC) of 0.68 [*Mosquera et al.*, 2015]. *Correa et al.* [2016] evaluated individual rainfall-runoff events in the same study area and derived from this information a median RC of 0.80, indicating that an even higher proportion of water in the active catchment storages is quickly released during rainfall events.

Table 1. Physiographic Characteristics of the Catchment

Physiographic Characteristics	Unit	Value
Area	km^2	7.6
Altitude avg.	m asl	3700
Slope avg.	%	17
Mainstream length	km	4.6
Drainage density	km km^{-2}	3.2
Drainage slope	%	1.9
Topographic wetness index (TWI)		16.7
Distribution of soil types	Andosols %	72
	Histosols %	24
	Leptosols %	4
Land cover	Tussock grass %	72
	Cushion plants %	24
	Polylepis forest %	2
	Pine forest %	2
Land use	Natural %	57
	Extensive grazed %	37
	Intensive grazed %	2
	Forest %	4
Geology	Quimsacocha %	56
	Turi %	31
	Quaternary deposits %	13

The geology of the basin belongs to the Quimsacocha (basalt flows with plagioclase, feldspat and andesitic pyroclastic deposits) [*Pratt et al.*, 1997] and Turi Formations (accumulation of a thick sequence of conglomerates, fluvial sands, clays, tuffs, and volcanic breccia) [*Coltorti and Ollier*, 2000] (Table 1). Quaternary formations were deposited during the glacial activity of the last Ice Age and cover 13% of the catchment area.

Histosols (24%) and Andosols (72%) are the dominant soils in the basin, which are characterized by low mechanical strength. These soils are strongly acidic with pH values around 4.8. The soils in the catchment are highly porous and possess a high retention capacity for water. The top layer of the Andosols averages 44 cm thick [*Quichimbo et al.*, 2012]. The top horizons of the Histosols

are histic, containing a high fraction of nondecomposed plant fibers [*Beck et al*., 2008], and have an average depth of 33 cm [*Quichimbo et al*., 2012]. The organic-rich Histosols are primarily located at the foot of the hillslopes and in the valley bottoms and are commonly covered by cushion plants and *Polylepis* trees. The more freely draining Andosols are situated on the hillslopes under a cover of tussock grass.

The land cover is relatively undisturbed with species such as tussock grass (72% of the catchment area) and cushion plants (24%) in the central and northeastern areas of the catchment. Riparian forests species such as *Polylepis incana* Kunth and *Polylepis reticulata* Kunth cover 2% of the basin. The remaining 2% are intermittent plots that are planted with pine trees.

3. Data and Methods

3.1. Hydroclimatic Data

The discharge station was equipped with a Schlumberger Diver water-level sensor, which has a precision of ±5 mm and measures the water level at 5 min intervals. The theoretical Kindsvater-Shen equation, which was adjusted by manual discharge measurements, was used to convert the water level to streamflow. The discharge values of Q35 and Q90 (frequency of nonexceedance based on flow duration curves), which were determined by *Mosquera et al*. [2015], were used as thresholds for the classification of flow rates. Low-flow rates were those below Q35, flow rates between Q35 and Q90 were classified as moderate, and high-flow rates were runoff values above Q90.

The precipitation network consisted of four fully automatic tipping-bucket rain gauges (0.2 mm resolution) across the catchment. The measured precipitation time series were corrected by *Padrón et al*. [2015] to account for drizzles (+15%). After this correction, the area-weighted precipitation for the entire catchment was calculated by applying the Thiessen polygon method, yielding an average annual value of 1300 mm for our study period. A summary of the hydroclimatic characteristics is shown in Table 2.

For the interpretation of the results a distinction was made between the less rainy months, from July to October (covering the 4 consecutive months with the lowest amount of rainfall, with mean rainfall rates of 52 mm per month in 2012 and 76 mm per month in 2013), and the rainy months between November and June (mean rainfall rates of 151 mm per month in 2012 and 110 mm per month in 2013). We refer to these periods as the *drier* and *wetter* seasons, respectively.

3.2. Water Sampling Design and Field Collection

The monitoring sites were selected to capture as much of the catchment's heterogeneity as possible (e.g., geology, geomorphology, soils, or land-cover types) and the origins of flow components, as reflected in the signals of the environmental tracers [*Barthold et al*., 2011]. Twelve potential sources and stream waters were monitored from April 2012 to April 2014, including the rainfall, soil water in an Andosol and two Histosols at three depths, spring water, and overland flow (Figure 1).

Rainwater samples were collected by using circular funnels (diameter = 16 cm) that were connected to polypropylene collectors to analyze the element concentrations. Similar collectors were used for stable isotopes, but these devices were covered with aluminum foil, a 0.5 cm layer of mineral oil was placed on top of the collected water, and plastic spheres were placed inside the funnels to prevent evaporation. An extensive description of the sample collection procedure is available in *Mosquera et al*. [2016a]. Both collection devices were placed next to a tipping-bucket gauge that recorded the rainfall (RF).

Table 2. Hydroclimatic Characterization of the Zhurucay Basin 2012–2014

Precipitation[a] (mm yr^{-1})	Total Runoff[a] (mm yr^{-1})	Runoff Coefficient	Specific Discharge[a] (L s^{-1} km^{-2})	Average Time to Peak[b] (h)	Relative Humidity[a] (%)	Temperature[a] (°C)
1300	828	0.64	26.2	6.6	92.7	6
Flow Rates, as Frequency of Nonexceedance (L s^{-1} km^{-2})						
Qmin	Q10	Q30	Q50	Q70	Q90	Qmax
2.2	5.6	9.0	13.0	20.9	44.9	695.7

[a]Average annual values.
[b]Time from the beginning of the rising limb to the occurrence of the peak discharge.

Soil water in an Andosol along a hillslope was collected at 0.25, 0.35, and 0.65 m below the surface (IDs = AN1.1, AN1.2, and AN1.3); the first two depths were at a horizon with high organic matter content and the third depth was at an organic mineral interface horizon. The soil water samples in the Histosol soil were collected at two sites: HS1 near the valley bottom and HS2 in a confined wetland on a flat hilltop in the northeast of the catchment. Water samples were collected at three depths, namely, 0.25, 0.45, and 0.75 m below the surface (IDs = HS1.1, HS1.2, and HS1.3 and HS2.1, HS2.2, and HS2.3). The slope at HS1 was slightly higher than that at HS2. Following the methodology of *Boll et al*. [1992], wick samplers were installed to collect soil water.

Spring water (SW, Figure 1) was included in the monitoring since April 2013 based on the distinct differences in the electrical conductivity with local stream, namely, 116 versus 63 $\mu S\ cm^{-1}$.

Overland flow (OF) rarely occurred but was observed at a few occasions after long and intense precipitation when the soils exceeded saturation. Three times OF samples were collected at five locations (Figure 1) in April 2014 by using handmade devices that consisted of a 100 cm-long and 10 cm-diameter polypropylene container that was cut over a length of approximately 3 cm (avoiding contamination from rain water), closed at one end and connected to bottles through funnels at the other end.

Stable water isotope samples were filtered *in-situ* through 0.45 μm polypropylene membrane filters (Puradisc 25PP Whatman Inc., Clifton, NJ) to minimize organic matter contamination. The isotope samples were stored in 2 mL amber glass bottles and sealed with screw caps with silicon septa. The bottles were covered with parafilm and placed in a dark container to avoid evaporative fractionation and the incidence of sunlight.

Samples for element analysis by inductively coupled plasma-mass spectrometry (ICP-MS) were filtered *in-situ* (0.45 μm polypropylene membrane filters, Puradisc 25PP Whatman Inc., Clifton, NJ), stored in acid-washed 100 mL polypropylene bottles, and acidified to $pH < 2$ with purified nitric acid to avoid trace metal precipitation and adsorption during storage.

The electrical conductivity (EC) and pH were measured *in-situ* by using a handheld multiparameter instrument (pH/Cond 340i, WTW, Weilheim, Germany) with a precision of 0.1 $\mu S\ cm^{-1}$. The EC was corrected by nonlinear temperature compensation at 25°C, and the pH was measured by using two pH electrodes, specifically, a SenTix 980 digital IDS and a SenTix HW pH electrode, for low-conducting samples.

Water samples for stable isotope analysis were collected weekly and element-concentration samples were collected biweekly, including event sampling in the main stream (Figure 1) and potential runoff sources. The EC and pH were measured at the time of sample collection.

3.3. Laboratory Analysis

The water isotopic composition was determined at the University of Cuenca with a wavelength-scanned cavity ring-down spectrometer (Picarro L1102-I, Sunnyvale, CA). Conforming to the manufacturer's specifications, the precision for $\delta^{18}O$ and $\delta^{2}H$ was $\pm 0.1‰$ and $\pm 0.5‰$, respectively. Starting from October 2013, all the results were processed by using the ChemCorrect 1.2.0 software (Picarro, Sunnyvale, CA) [*Picarro*, 2010]. Two samples with high organic contamination were excluded from further analysis. The results were reported in per mil (‰) units relative to the Vienna Standard Mean Ocean Water (VSMOW) indicator.

The concentration of 22 elements, including rare earth trace elements (Li, Na, Mg, Al, Si, K, Ca, Fe, Mn, Ni, Cu, Zn, Rb, Sr, Ba, Ce, V, Cr, Y, As, Nd, and U), were determined at the Institute for Landscape Ecology and Resource Management of the Justus Liebig University of Giessen by using the ICP-MS analytical technique (Agilent 7500ce, Agilent Technologies). The quality of the measurements was controlled by certified reference material (NIST 1643e – SLRS4 and NIST 1640e – SPSSW2) and internal calibration standards. The inclusion of rare earth trace elements was based on previous studies, where the authors highlighted the importance of those elements in the definition of water sources [*Bücker et al*., 2010]. The results were reported as parts per billion (ppb), representing the mean of two consecutive measurements.

3.4. Data Analysis

A hydroclimatic description, chemical and isotopic characterization of the collected data (first objective) was performed to conceptualize the uniqueness of each catchment source/sampling site (presented in section 4.1), followed by an EMMA to study the dominant sources of runoff generation (second objective) and

a multimethod analysis that was based on EMMA, hydrograph separation, and ITTPs to assess the temporal response of the water sources, dynamics in flow paths and water ages (third objective).

3.4.1. End Member Mixing Analysis (EMMA)

End-members are defined as functional units of catchments and represent the water sources that physically mix during translocation to the stream channel [*James and Roulet*, 2006]. The recommendations of *Christophersen and Hooper* [1992] and *Hooper* [2003] were followed during the application of the EMMA method, including (1) the identification of conservative tracers (not involved in adsorption or biological processes); (2) a principal component analysis (PCA) and residual error analyses to determine the dimensionality of the hydrologic system; (3) the identification of the best fit end-members (dimensionality + 1); and (4) the computation of the contribution from each end-member to the streamflow.

1. A set of 22 elements, EC and pH from stream data were tested to identify conservative tracers. First, the outliers of each tracer (in our case, values 1.5 times from the interquartile range) were removed. Bivariate scatter plots (tracers versus tracer) were developed for all possible combinations, and the related R^2 and *p*-values were calculated. A collinear structure in the plots and a R^2 value >0.5 (p-value < 0.01) were used to consider a tracer as conservative [*Hooper*, 2003; *James and Roulet*, 2006]. After assessing the bivariate plots, R^2 values and *p*-values, 14 tracers (Na, K, Rb, Ba, Ca, Sr, Mg, Si, Al, V, Y, Ce, Nd, and EC) were identified as conservative (the data that were used are presented as supporting information).
2. A PCA with stream data (total stream data set) was applied to identify a subdimensional U-mixing space that explains most of the variation in the identified conservative tracers. A procedure by *Hooper* [2003] was used, including a residual error analysis and the calculation of the Relative root-mean-square error (RRMSE) between the stream water tracer concentrations and their orthogonal projections in the different subspaces to evaluate the fit of these data in a mixing subspace as defined by their own eigenvectors. The dimension of the mixing subspace is defined by small RRMSE values and the smallest possible space where all plots (residuals against the original concentration) appear to be random [*Hooper*, 2003; *James and Roulet*, 2006]. Additionally, the residuals were evaluated in light of the analytical precision. Patterns in the plots disappeared and the RRMSE values (Table 3) decreased for all the tracers in the third and higher dimensional subspaces. Thus, we used a third mixing space dimension for further analysis.
3. The medians and standard deviations of all potential end-members were orthogonally projected into the mixing subspaces as defined by the PCA of the stream samples. End-members were selected based on their ability to enclose the stream concentrations in the U3-space. Ideally, end-member solutions should exhibit extreme chemical concentrations compared to stream water, low variability compared to the stream chemistry and exhibit distinctive concentrations between end-members [*Hooper*, 2001].
4. The percentage of the contribution from each end-member to the streamflow was computed by solving the set of linear equations that was proposed by *Christophersen et al*. [1990] (equations (1)–(4)). The mixing-model theory was applied by *Christophersen and Hooper* [1992] to state that stream samples are a linear mixture of the fraction of end-members that form a convex polygon, where the fractions are nonnegative and sum to 1:

$$1 = a_1 + a_2 + a_3 + a_4 \tag{1}$$

$$SW_{U1} = a_1 EM1_{U1} + a_2 EM2_{U1} + a_3 EM3_{U1} + a_4 EM4_{U1} \tag{2}$$

$$SW_{U2} = a_1 EM1_{U2} + a_2 EM2_{U2} + a_3 EM3_{U2} + a_4 EM4_{U2} \tag{3}$$

$$SW_{U3} = a_1 EM1_{U3} + a_2 EM2_{U3} + a_3 EM3_{U3} + a_4 EM4_{U3} \tag{4}$$

Table 3. Relative Root-Mean-Square Error for Projection of Stream Water Observations in a Mixing Subspace Created by Its Own Eigenvectors

Dimensionality[a]	Na	K	Rb	Ba	Ca	Sr	Mg	Si	EC	Al	V	Y	Ce	Nd
1	0.006	0.015	0.014	0.008	0.012	0.009	0.008	0.011	0.01	0.032	0.016	0.022	0.033	0.026
2	0.006	0.013	0.009	0.008	0.011	0.007	0.007	0.011	0.009	0.017	0.011	0.013	0.024	0.011
3	0.006	0.008	0.006	0.004	0.011	0.007	0.005	0.011	0.007	0.014	0.011	0.010	0.019	0.010
4	0.005	0.008	0.005	0.004	0.010	0.006	0.005	0.011	0.007	0.014	0.011	0.008	0.018	0.009

[a]RRMSE values from the first four dimensions.

where a_1, a_2, a_3, and a_4 are the fractions of the four end-members; SW_{U1}, SW_{U2}, and SW_{U3} are the projected stream water observations in the U-space (mixing subspace) coordinates; and EMn_{U1}, EMn_{U2} and EMn_{U3} (n1–4) are the coefficients of the nth end-member as projected in the U-space.

Stream observations that lie outside the domain that is defined by the selected end-members (negative fraction) because of input-data uncertainty or time-dependent end-member variability [*Christophersen and Hooper*, 1992; *Chaves et al*., 2008] were projected onto the plane that excluded the end-member with a negative contribution, forcing the negative fraction to be zero, and the other contributions were assumed to be a mixture of the remaining end-members [*Liu et al*., 2004] (see Appendix A). Additionally, the quality of the selected end-members was determined in terms of the good fit between the observed and predicted stream concentrations for each solute. The predicted stream concentrations were calculated as the matrix product of the contributions from every end-member for each stream observation and the projected end-member medians in terms of the original solutes following *Christophersen and Hooper* [1992] and *Hooper* [2003].

3.4.2. Two-Component Hydrograph Separation

Although two stable water isotopes, namely, δ^{18}O and δ^{2}H, were monitored, we only used δ^{18}O for further analysis, which is in accordance with *Mosquera et al*. [2016a], who stated that both isotopes yield comparable results. Variations in the isotopic content of weighted precipitation and stream water permitted the use of a simple mass balance approach to separate hydrographs into its event and preevent components. Weekly isotopic δ^{18}O time series were used as input data (the data that were used are presented as supporting information). The preevent signature in the streamflow was defined as the previous day streamflow signature [*Tetzlaff et al*., 2014]. We adapted this concept to our time-scale resolution (previous week):

$$\frac{Q_{pre}}{Q_t} = \frac{\delta_e - \delta_t}{\delta_e - \delta_{pre}} \tag{5}$$

where Q_{pre} is the preevent contribution to the total discharge Q_t; δ_e (‰) and δ_t (‰) are the observed event signature in the precipitation and streamflow, respectively; and δ_{pre} is the preevent signature in the streamflow. Altitudinal effects on the isotopic composition of precipitation were reported in the region [*Windhorst et al*., 2013; *Mosquera et al*., 2016a]. Consequently, the isotopic signature of precipitation (δ_e) was corrected by $-0.31‰$ per 100 m elevation increase according to *Mosquera et al*. [2016a]. The Gaussian error propagation technique by *Genereux* [1998] was applied to compute the total uncertainty in the hydrograph separation. The uncertainty terms (stream water, new water and old water) for the weekly hydrograph separation are all based on a single sample, using an instrumental precision of $\pm 0.1‰$ δ^{18}O instead of the standard deviation [*Liu et al*., 2004], and weighted by multiplying this value with the asymptotic Student's t value [*Genereux*, 1998] at a confidence level of 95%.

3.4.3. Inverse Transit Time Proxies (ITTPs) for the Different Sources

ITTPs are based on a simple measure of tracer damping, which is calculated as the ratio of the standard deviation of δ^{18}O in stream water to the standard deviation of δ^{18}O in precipitation [*Tetzlaff et al*., 2009]. In previous studies, ITTPs were shown to be proportional to the MTT estimates [*Tetzlaff et al*., 2009; *Capell et al*., 2012; *Seeger and Weiler*, 2014]; stronger damping indicates longer MTTs. *Birkel et al*. [2016] presented ITTPs as a strong predictor of MTT with an exponential relationship of $R^2 = 0.59$. In our study, we correlated published MTT values of seven tributaries and the main stream [*Mosquera et al*., 2016b] with ITTPs that were derived from the corresponding isotope time series to verify the feasibility of using the ITTPs approach as an indicator of MTT. We found good agreement between both indicators with a determination coefficient of 0.85 ($p < 0.01$). After verification, the same concept (measure of tracer damping) was applied for δ^{18}O isotope time series from different water sources.

An 8 week moving window was applied to the δ^{18}O isotope time series to calculate the ITTPs of different water sources (1 week time step). The time of the window was estimated by the shifts in the isotope peaks of the precipitation inputs and source-water outputs during extreme events. During this period, consecutive peaks in the rainfall-isotope time series, one depleted and one enriched, were observed in all cases. Here $\pm 50\%$ of the estimated time window was used as an error band to explain the uncertainty.

4. Results

4.1. Hydroclimatic, Hydrochemical, and Isotopic Characterization

Our analysis of the hydrograph indicated that close to 10% of the recorded flow rates were high, 55% of the flow rates were moderate and 35% were low during the study period (Q90 = 45 L s^{-1} km^{-2} and

Q35 = 10 L s^{-1} km^{-2} were used as thresholds). The low flows were mainly observed during two periods: July–October 2012 and October–December 2013. The annual amount of streamflow varied between 915 (2012) and 740 mm (2013), consistent with the annual precipitation, which varied from 1420 to 1180 mm yr^{-1} during the same period. High precipitation intensities (>0.5 mm h^{-1}) were registered between October and June, representing 0.3% of the events, and a maximum value of 13 mm h^{-1} was observed in December 2013. The most common recorded intensity was 0.061 mm h^{-1}.

The median and standard deviation values of geochemical tracers from the stream and potential end-members are depicted in Figure 2. The tracers were grouped according to similar tendencies in the median source values among the elements, including alkali and alkaline earth metals (Na, K, Rb, Ba, Ca, Sr, and Mg) and semimetals (Si) as Group 1 (G1) and transition elements, including Al, as Group 2 (G2). The median EC values showed comparable behavior to the elements in G1, so this variable was included in this group. The EC of stream water, which had a median value of 28 μS cm^{-1}, showed the greatest similarities to the HS1.1 (29.9 μS cm^{-1}) and OF values (27.6 μS cm^{-1}).

RF depicted the lowest values for G1 compared to stream water and other potential end-members (Figure 2). In G1, the median values for RF and water from AN1.1 were similar, while RF was in the range of SW and OF in G2. Rare earth elements in RF were one order of magnitude lower than in stream water. The Andosols presented generally lower median concentrations of all soil sources, except for the different patterns that were observed for K and Rb. For G1, HS1 had higher average values than HS2; the latter displayed the highest median concentration for the elements in G2, while SW displayed the highest value in G1. The SW (G1) values were around 4 times higher than the concentrations of those elements in stream water.

Horizon analyses revealed that the solute concentrations of G1 in the Andosols increased with depth, in contrast to the behavior of the G2 elements. For HS1, the most diluted water was originated from a depth

		Na	K	Rb	Ba	Ca	Sr	Mg	Si	EC	Al	V	Y	Ce	Nd
Stream	Median	2235.3	853.4	2.0	24.4	2573.7	47.4	366.2	6275.9	28.0	98.4	0.47	0.10	0.12	0.11
n=146	Std	780.7	253.6	0.4	3.9	748.3	15.5	115.7	1949.9	9.0	46.3	0.17	0.02	0.06	0.04
RF	Median	91.7	319.8	0.2	2.6	240.8	1.1	33.1	33.0	7.3	77.8	0.26	0.01	0.03	0.02
n=54	Std	39.7	149.7	0.2	1.6	120.8	0.6	19.1	27.3	2.0	62.2	0.15	0.01	0.02	0.01
AN1.1	Median	156.2	491.9	1.4	4.6	479.2	5.6	96.4	2081.2	7.5	288.3	0.62	0.08	0.26	0.14
n=54	Std	62.5	386.8	0.9	1.2	168.0	0.8	17.6	318.7	1.8	85.3	0.13	0.01	0.07	0.02
AN1.2	Median	288.5	1087.6	2.7	9.9	581.7	8.1	137.9	2258.6	15.1	250.9	0.46	0.06	0.19	0.10
n=57	Std	69.8	181.1	0.4	3.2	217.4	2.4	33.5	433.8	2.7	94.2	0.11	0.02	0.09	0.03
AN1.3	Median	537.0	934.6	1.2	36.4	926.9	24.3	207.6	2813.3	17.3	148.4	0.24	0.02	0.05	0.03
n=58	Std	148.1	470.0	0.5	10.3	383.7	12.3	80.5	516.0	3.4	65.2	0.07	0.03	0.01	0.02
HS1.1	Median	2041.1	1094.7	2.6	26.8	3034.9	49.1	361.4	7809.0	29.9	162.5	0.32	0.09	0.15	0.14
n=20	Std	336.7	485.1	1.3	6.9	531.4	7.5	39.6	706.2	4.0	72.8	0.13	0.03	0.04	0.04
HS1.2	Median	1861.5	400.1	1.8	30.5	2560.7	45.9	337.0	6814.4	31.4	148.6	0.29	0.08	0.18	0.13
n=56	Std	198.3	235.1	0.4	7.8	607.7	10.1	43.5	1020.8	4.3	61.1	0.16	0.03	0.07	0.04
HS1.3	Median	2262.1	1404.7	4.8	22.5	3174.8	56.1	529.0	7019.2	38.4	185.2	0.29	0.17	0.24	0.18
n=46	Std	296.1	256.3	1.2	6.2	1143.6	18.5	204.6	784.7	5.0	125.8	0.17	0.04	0.07	0.04
HS2.1	Median	1164.8	275.8	0.5	25.6	2248.2	32.9	368.1	3244.3	19.4	617.1	0.60	0.20	0.44	0.40
n=17	Std	360.7	94.8	0.2	3.6	556.9	5.2	43.6	562.0	3.6	163.5	0.19	0.05	0.11	0.19
HS2.2	Median	1059.5	406.5	0.9	12.0	1455.6	17.8	484.7	4697.3	23.5	379.1	0.76	0.38	0.66	0.41
n=17	Std	193.5	316.2	0.8	5.3	363.1	1.5	128.2	1175.6	6.9	738.8	0.60	0.13	0.32	0.12
HS2.3	Median	2146.8	905.7	1.4	35.7	1530.6	18.5	475.0	7145.3	23.4	3025.5	4.35	0.39	0.72	0.60
n=10	Std	327.3	198.2	0.1	9.9	635.0	4.2	99.7	1222.7	1.5	828.6	1.58	0.13	0.30	0.19
[a]SW	Median	7252.1	2855.4	6.0	69.5	11513.2	196.3	2525.4	22405.4	115.5	36.6	1.62	0.01	0.03	0.01
n=28	Std	545.8	243.3	0.5	4.3	901.4	8.0	128.1	3323.2	4.7	20.6	0.09	0.02	0.01	0.01
[b]OF	Median	1704.4	710.5	0.9	27.7	2298.3	42.0	244.0	5129.1	27.6	40.5	0.10	0.01	0.01	0.02
n=15	Std	580.1	283.8	0.5	7.6	577.4	11.8	44.6	1447.8	6.8	20.4	0.08	0.01	0.02	0.02

Figure 2. Tracers characterization, median, and standard deviation of stream and potential end-members for the study period 2012–2014. RF, rainfall; AN, Andosols; HS, Histosols; x.1–x.3, three soil depths; SW, spring water; OF, overland flow. Element concentrations in (ppb) and EC in (μS cm^{-1}). Three-color scale represents: red for maximum, yellow for midpoint, and green for minimum. [a]SW from 2013 to 2014; [b]OF in April 2014.

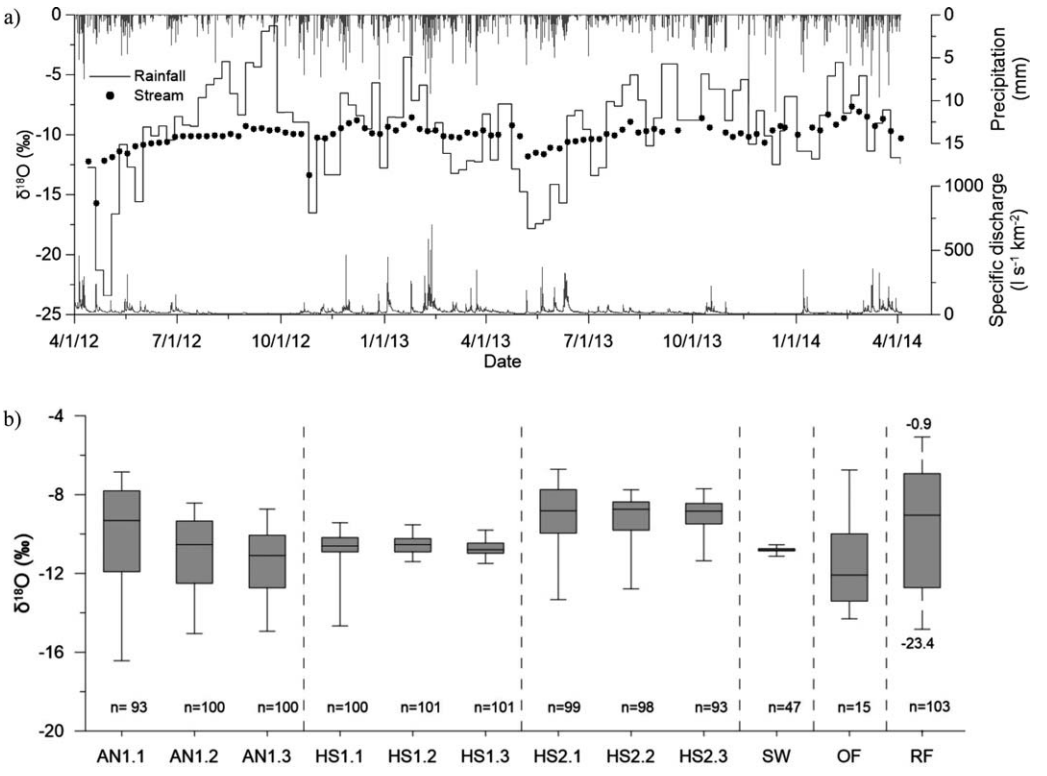

Figure 3. (a) Dynamics of the weekly isotope signatures of rainfall and stream water, specific discharge, and precipitation time series; (b) box plots of isotopic δ^{18}O composition of potential water sources (the central bar in the box represents the median; notches represent the maximum and minimum value and the length of the box indicates the interquartile range). AN, Andosols; HS, Histosols; x.1–x.3, three soil depths; SW, spring water; OF, overland flow; RF, rainfall. Dotted lines separate water source types.

of 0.35 m below the surface. HS1 and HS2 did not exhibit a clear trend of either high or low concentrations. Nevertheless, an overall higher concentration of elements could be observed in the deeper horizons of all the soils.

The isotope signal of rainfall varied from $-23.4‰$ to $-0.9‰$, with lower δ^{18}O values observed during May and June (lower than $-14.0‰$) and higher δ^{18}O values (higher than $-5.0‰$) in August and September (Figure 3a), when the lowest temperature values were recorded. The streamflow variations were attenuated but still showed a high responsiveness to the input of rainfall. The isotopic composition ranged from $-7.6‰$ to $-15.7‰$, following a comparable pattern of the rainfall. The median values of the rainfall and stream isotope data were similar (–9.04‰ and $-9.93‰$, respectively), but a fourfold higher standard deviation was observed for the precipitation.

The isotopic composition of soil water considerably varied, with Andosols exhibiting a higher variability than Histosols and higher δ^{18}O values in the more porous top soil (Figure 3b). The horizons of the HS1 profile showed the most stable behavior in the signature and were the least responsive to rainfall, with median values between $-10.5‰$ and $-10.8‰$ (Figure 3b). This source exhibited the most similar signature to stream water.

HS2 showed a higher variability than HS1 and the highest δ^{18}O median values of all the soil sources. The SW signature revealed the greatest damping behavior, with an isotopic composition from $-10.5‰$ to $-11.1‰$. OF presented maximum and minimum values within the range of those in the upper Andosol and Histosol soil horizons and showed the lowest δ^{18}O median values of all the sources.

4.2. Sources of Runoff

The PCA of the stream water data explained 60.2% of the variance for the first principal component (U1), 18.4% for the second (U2), and 6.9% for the third (U3). The median values and standard deviations of the end-members projected into the U3-space of the stream water are shown in Figures 4a–4c.

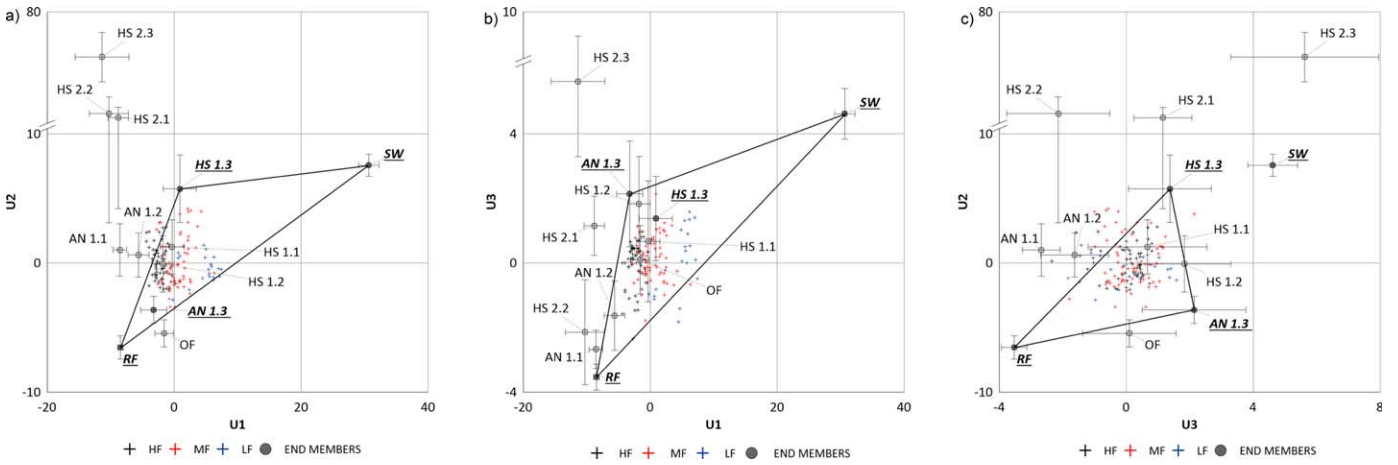

Figure 4. Mixing subspaces generated from the main stream water samples: (a) mixing subspace U1–U2; (b) mixing subspace U1–U3; and (c) mixing subspace U2–U3. U1 represents 60.2% of the variance, U2 18.4%, and U3 6.9%. HF, high flows (HF > Q90); MF, moderate flows (Q35 > MF < Q90); LW, low flows (Q35 > LF); RF, rainfall; AN, Andosols; HS, Histosols; x.1–x.3, three soil depths; SW, spring water; OF, overland flow.

U1 mostly explained the variability in the fresh and old water in the system. RF was located on the left side of the stream cloud and SW on the right side (Figure 4); the patterns of the sources' contributions to the streamflow were depicted in this component (Figures 4a and 4b). The composition of high flow tended to range between RF and Andosols and low flow between Histosols and SW. All the soil horizons from AN1 and HS1 were located between RF and SW.

A large variation in the chemical composition between HS2 and the stream data was observed in U2 and U3 (Figure 4). HS2 plotted far away without enclosing stream observations. In U2 differences in chemical composition between AN1.3 and HS1.3 were identified, while the upper horizons from AN1 and HS1 plotted very close to each other. Infiltration processes throughout the Andosols horizons could be inferred in U3 because the upper horizon plotted near the RF source and progressively deeper horizons became chemically enriched. The median value of OF was located close to HS1.1 and fell within the stream data cloud in the subspace U1–U3.

According to the above mentioned methodology, the most suitable set of four end-members consisted of RF, SW and water from the bottom horizons of two different soil types (Histosols and Andosols). Most of the stream water observations fell into the domain that was defined by the selected end-members, a tetrahedron in our case. SW represented water with a long contact time with the bedrock material, showing higher solute concentrations from other sources. Although the SW median plotted relative far from the stream water cloud (Figure 4), this value was an essential extreme to define the space that enclosed the stream observations. Satisfactory quality was found for the end-members, with Pearson coefficients between the observed and predicted stream concentrations, specifically, between 0.98 and 0.78 ($p < 0.01$). The slope of the regression lines varied from 0.9 to 1.2.

4.3. Temporal Dynamics in Runoff Sources, Flow Paths, and Transit Time Proxies

In terms of investigating variations in source contributions depending on the hydroclimate conditions, a comparison between the relative contributions to the stream and the specific discharge showed a clear trend for SW (Figure 5), whose contribution potentially decreased with higher specific discharge ($Y = 1.48X^{-0.8}$). On the contrary, no clear relationships were found for RF, AN1.3 or HS1.3 and the specific discharge. Only slight trends in stabilizing their contributions with higher specific discharge were observed (Figure 5). To clarify these tendencies, an analysis of the median percentage of the contributions of every end-member was conducted under different flow conditions and during wetter and drier periods.

Under low-flow conditions, HS1.3 and SW contributed the highest proportions to the specific discharge (34% and 31%, respectively; Figure 5), followed by RF (22%) and AN1.3 (13%). Under moderate-flow conditions, the contribution from RF increased to 29%, while the contribution from the soils rose to 40% for HS1.3 and 18% for AN1.3. The contribution from SW decreased to 13%. Under high-flow conditions, HS1.3's

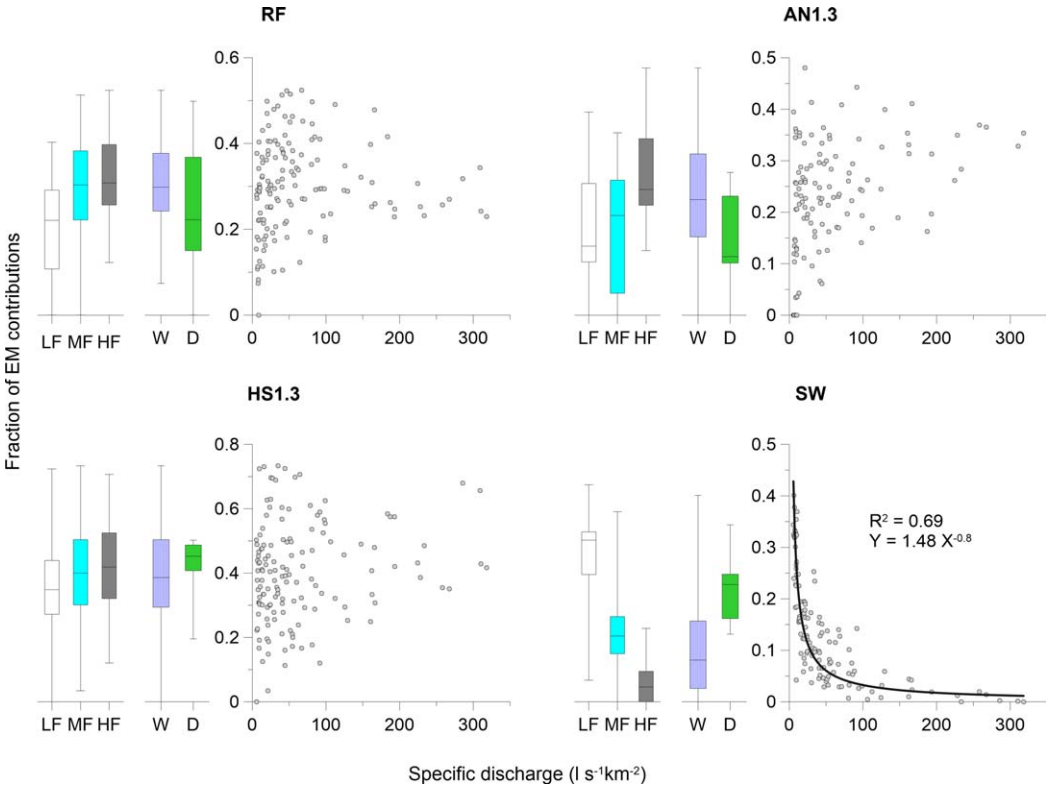

Figure 5. Fraction of the end-member contributions versus the specific discharge and box plots of end-member contributions during different flow conditions in wetter (W) and drier (D) seasons (the central bar in the box represents the sample median; notches represent the maximum and minimum value and the length of the box indicates the interquartile range). RF, rainfall; AN1.3, Andosol, third soil layer; HS1.3, Histosol, third soil layer; SW, spring water; HF, high flows (HF > Q90); MF, moderate flows (Q35 > MF < Q90); LW, low flows (Q35 > LF). Y represents the fraction of end-member contribution and X the specific discharge.

contribution increased (42%) and SW's contribution continuously decreased (3%), while the remaining sources displayed contributions of 31% for RF and 24% for AN1.3.

A seasonal analysis revealed that the contribution from RF to the specific discharge slightly decreased from 30% in the wetter season to 22% in the drier season (Figure 5). HS1.3 and SW contributed more to the discharge during the drier season (45% and 23%, respectively), decreasing to 39% and 8% in the wetter season. The median contribution from AN1.3 was nearly two times higher during the wetter season (23%).

The isotope-based two-component hydrograph separation showed that preevent water was the major component of the streamflow. Most of the time, the fraction of preevent water was higher than 75% (Figure 6a). Preevent water was 10% higher during the drier season than the wetter season, averaging 94% and 84%, respectively. The percentage of preevent water exhibited lower values during the wetter season, occasionally dropping to less than 50%. However, no specific type of runoff event or flow condition could be related to the lower preevent water component. The uncertainty in the hydrograph separation results ranged from $\pm$2% to $\pm$63% and averaged $\pm$13.5% (Q10 = 4% and Q90 = 27%).

The median values of the ITTPs from the stream data (Figures 6b and 6c) showed slight seasonal variation. As Table 4 shows, higher median values were obtained from the wetter season compared to the drier season (0.24 and 0.13, respectively). During wet periods, the ITTPs time series of stream water and Andosols (Figure 6b) were particularly close. Relatively older Andosol soil water (at a depth of 0.25 and 0.35 m) appeared during the wetter season. The closest plot of Andosols to the streamflow was that with deeper horizon soil water (Figure 6b). SW did not exhibit obvious seasonal changes. During the drier season, the stream water was more similar to HS1 (Figure 6c). The high variability in the ITTPs series of water from HS2 (figure not shown) made the delineation of any clear tendency in relation to stream water difficult.

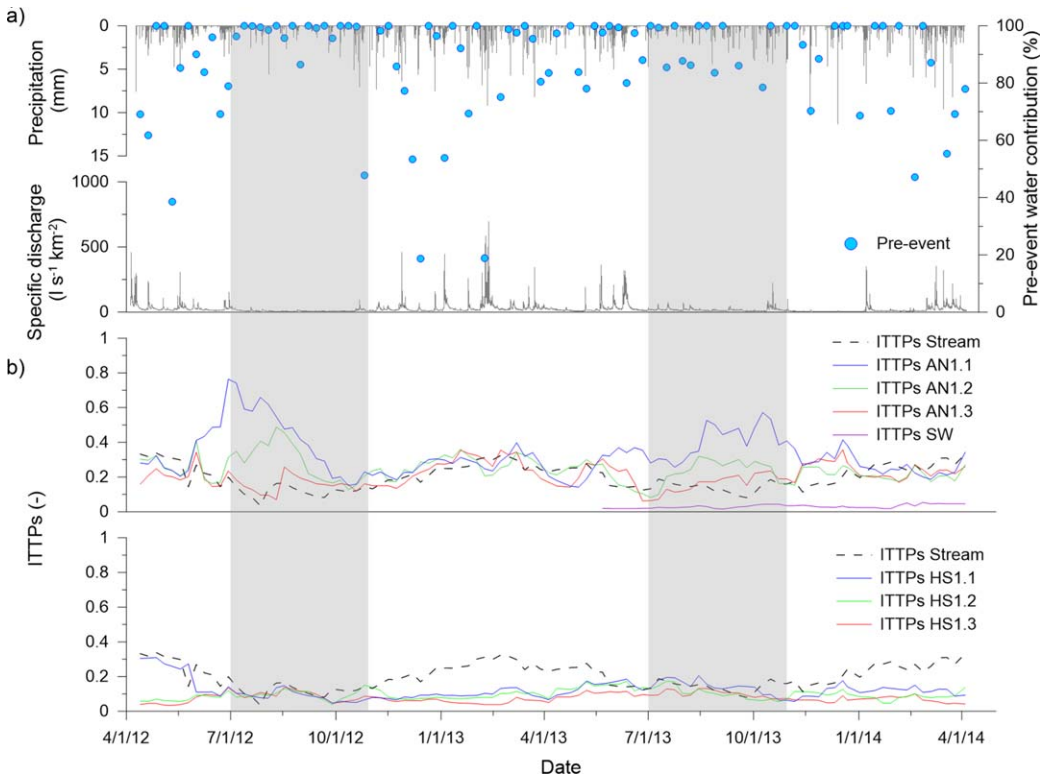

Figure 6. (a) Preevent water contributions based on a two-component isotopic hydrograph separation. Blue dots depict the fraction of preevent water contribution; (b) time series of Inverse Transit Time Proxies (ITTPs) for AN1.1, AN1.2, and AN1.3 representing the three sampled soil depths (0.25, 0.35, and 0.65 m) at the Andosol site and SW spring water; and (c) time series of ITTPs for HS1.1, HS1.2, and HS1.3 representing the three soil depths (0.25, 0.45, and 0.75 m) at the Histosol site. The light grey shaded blocks highlight drier seasons.

Relatively small increases in the water age proxy could be noted with increasing soil depth (Table 4), except for HS2, when the second horizon exhibited relatively older ages than the deepest horizon. The OF source was not included in this analysis because the inadequate time of the sampling resolution did not permit ITTPs analysis.

The results from the error band's 4 and 12 week time window (results not shown) revealed that a shorter window yielded similar median ITTPs (±0.02 on average) but doubled the mean standard deviation (from 0.06 to 0.12 on average) regardless of the season, while a longer window yielded similar results for the median (±0.01 on average) and did not affect the mean standard deviation (0.06 for both cases).

Table 4. Median and Standard Deviation Derived From Inverse Transit Time Proxies (ITTPs) Using 8 Weeks as Time Frame[a]

	Wetter Season		Drier Season	
Sources	Median	Std	Median	Std
Stream	0.24	0.06	0.13	0.03
AN1.1	0.28	0.09	0.4	0.15
AN1.2	0.25	0.06	0.26	0.1
AN1.3	0.23	0.06	0.16	0.05
HS1.1	0.11	0.07	0.1	0.05
HS1.2	0.09	0.03	0.1	0.03
HS1.3	0.06	0.02	0.09	0.02
HS2.1	0.26	0.1	0.31	0.18
HS2.2	0.08	0.11	0.18	0.08
HS2.3	0.11	0.06	0.26	0.08
SW	0.03	0.01	0.03	0.01

[a]Values reported for stream water and different water sources correspond to wetter and drier seasons. AN, Andosols; HS, Histosols; x.1–x.3, three soil depths; SW, spring water.

5. Discussion

5.1. Sources of Runoff

Combination of several established methods, used to analyze the hydrological processes at the catchment scale, yielded for the Páramo unique system characteristics. Our findings are particularly interesting because they show the feasibility of the EMMA approach beyond the classical three end-member applications. Four end-members are necessary to encompass the mixing space that is generated by 2 years of stream information and to satisfactorily represent the hydrological

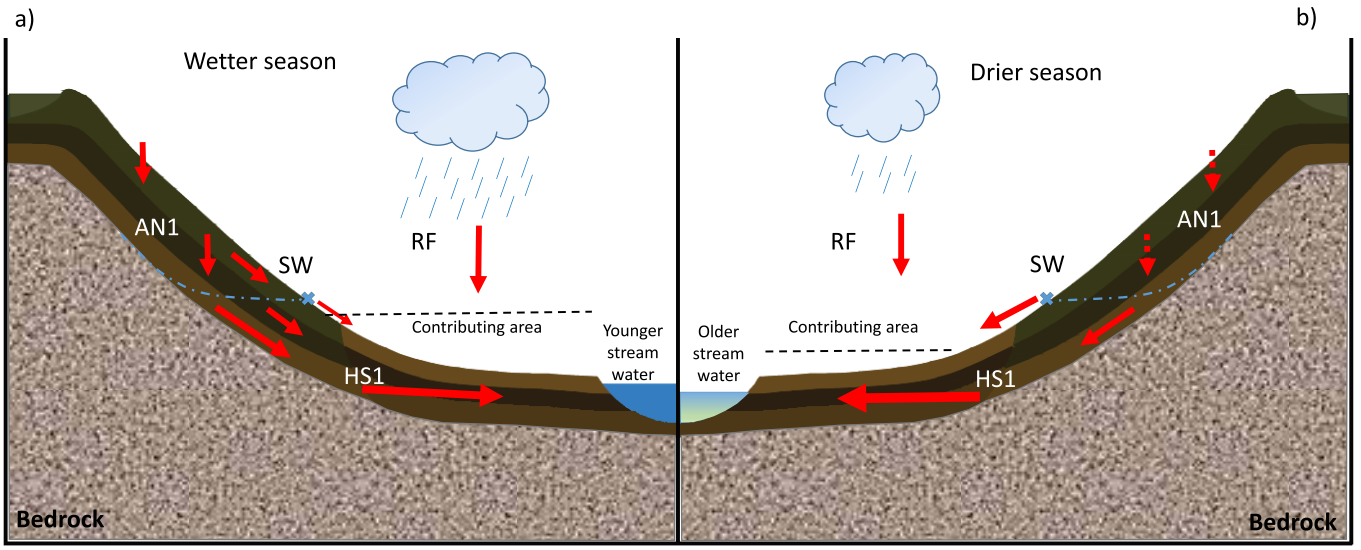

Figure 7. Conceptual model showing the relative contributions of the main water sources of runoff generation during the (a) wetter season (November–June) and (b) drier season (July–October). Red arrows, proportional contribution of each source to stream; dotted black line, varying extend of the contributing area; dotted blue line, bedrock-soil interaction; blue cross, location of spring water. AN1, Andosol; HS1, Histosol near valley bottom; RF, rainfall; SW, spring water. ITTPs values of 0.24 and 0.13 for younger and older stream water, respectively.

system of our study area. The selected end-members were RF, SW, and water from two different soil types, namely, AN1.3 on the hillslopes and HS1.3 near and in the valley bottom.

The possibility to identify a higher number of end-members increases when more tracers are available. A large set of tracers reduces the risk of incorrect conclusions regarding catchment functions [*Barthold et al.*, 2011]. Usually, authors limit their analysis to two or three end-members [*Katsuyama et al.*, 2001; *Ladouche et al.*, 2001; *Hugenschmidt et al.*, 2014; *Engel et al.*, 2016], even when a fourth end-member is required to explain the variance in stream water chemistry [*Ali et al.*, 2010]. Analyzing four or more end-member systems is more mathematically challenging, but this approach presents a more complete conceptualization of the mixing processes when applicable [*Lee and Krothe*, 2001; *Delsman et al.*, 2013; *Iwasaki et al.*, 2015; *Barthold et al.*, 2017]. The research findings by *Iwasaki et al.* [2015] highlighted the need for five end-members to consistently interpret the influence when studying the upscaling of storm-runoff generation processes in headwater catchments.

The fresh water that enters a system (RF) is an important source to runoff generation (22%–30%), suggesting direct channel precipitation [*Penna et al.*, 2015, 2016] and some shallow flow from the riparian area. The nearly saturated conditions of the riparian zone cause the storage capacity in these soils to be limited to the top centimeters of the upper soil horizon [*von Freyberg et al.*, 2014; *Mosquera et al.*, 2015]; consequently only a small fraction of rainfall can infiltrate [*Crespo et al.*, 2011]. This new water flows horizontally above the saturated zone in the Histosols and feeds the stream. A similar picture was presented by *Delsman et al.* [2013], who described how the water that entered their system only shortly interacted with the soil. *Barthold et al.* [2017] noted the importance of saturation-excess overland flow in their catchment, but their data suggested that this water was more likely new water. *Buytaert et al.* [2005, 2007] noted that a virtually impermeable bedrock in high Andean catchments minimized deep infiltration and that groundwater contributions were nearly absent. However, the implementation of tracer techniques enabled *Favier et al.* [2008] to pinpoint the influence of groundwater on stream generation. The novelty of using multitracer data sets from SW revealed the importance of shallow groundwater sources and the weathering of the mineral layers (rocks and soils) in our study area.

In accordance with our results, the essential role of shallow groundwater in headwater catchments was reported by *Shaw et al.* [2014] in California and high mountain catchments in Scotland with similar hydropedological conditions [*Blumstock et al.*, 2016]. In addition to our primary results regarding the relevance of shallow groundwater, detailed studies of its spatiotemporal variability are still required to better understand its contribution to runoff generation [*Lana-Renault et al.*, 2014; *Rinderer et al.*, 2014, 2016].

The water from Andosols underlined the importance of hillslopes in runoff generation, which should not be underestimated in catchment studies [*Iwasaki et al*., 2015] because of its important interaction with riparian zones [*Ali et al*., 2010] and relationship with the hydrological connectivity between uplands and streams [*Bergstrom et al*., 2016]. Based on our analysis, water from Andosols contributed to runoff primarily via the deeper soil horizons (AN1.3). Rainwater infiltrated through the upper porous horizon of the Andosols, percolated through the soil profile and obtained its chemical fingerprint (Figure 2), explaining the importance and usefulness of AN1.3 as a chemical end-member.

HS1.3 stands for water from the foot of the hillslopes, and the riparian zone seemed to exert an important influence on stream generation [*von Freyberg et al*., 2014], as suggested by plotting close to the stream water in the mixing subspace. Several studies in a range of catchments underlined the essential role of riparian soil water in runoff generation [*McGlynn and McDonnell*, 2003; *Jencso et al*., 2009; *Tetzlaff et al*., 2014; *Blumstock et al*., 2015].

Mosquera et al. [2016a] identified the shallow subsurface flow that occurs in the top layers of Histosols (HS1.1 and HS1.2) as one of the main discharge contributors based on the similarities in stable isotope signals between soil and stream water. In our study, all the HS1 horizons were active sources, but the top horizons plotted within the stream data lacking the condition of bound the stream water mixing cloud (Figure 4). These observations were a mixture of the distinct chemical signal of the Histosols (HS1.3) and water with a chemical signature closer to rainfall (RF) or Andosols (AN1.3). Additionally, we checked the set of end-members, selecting the upper Histosol horizons as end-members in our EMMA. The stream water's chemistry could also be explained, but in a lower proportion than the selected HS1.3 (Figure 4a). HS1.3 bounded the majority of stream water in the mixing cloud, satisfying the end-member condition to explain the highest mixture of stream water [*Christophersen and Hooper*, 1992]. Hence, our findings and those from *Mosquera et al*. [2016a] do not contradict each other, but rather, lead to the same conclusion, supporting that areas with similar chemical signatures to Histosols are important discharge sources in our study catchment.

Based on the location of the end-members in the mixing space of the EMMA approach, an additional end-member with a chemical signature between SW and HS1.3 could be missing. A mineral soil source below the lowest currently sampled Histosol horizon (HS1.3 at 0.75 m depth) could match this description. Such a source could also explain the long tail of the exponential model that was selected by *Mosquera et al*. [2016b] to describe the transition of the isotope signal and the currently important contribution from the monitored SW source. These discrepancies highlight the necessity to precisely consider the differences in methods when interpreting the contributions from different sources to flow generation.

5.2. Temporal Dynamics in Runoff Sources, Flow Paths, and Transit Time Proxies

The dynamics in the RF's contribution revealed this factor's importance under different flow conditions, increasing slightly from low to moderate flows. The contribution from AN1.3 and HS1.3 amplified from low to moderate and high-flow conditions, whereas the spring water's contribution considerably decreased when the discharge increased. In our seasonal analysis, water from Histosols was the main contributor to stream water year round; matching a hydrological system that is dominated by preevent water. During the drier season, stream water became enriched in solutes with higher contributions from springs. The ITTPs supported these findings, reflecting an increase in stream water age during drier periods and process connectivity within hillslopes under wet conditions.

Figure 7 depicts the conceptualization of our findings. The contributing area expanded when the flow level increased during rainfall-runoff events [*Beven and Kirkby*, 1979; *Correa et al*., 2016]. This expanded area increased the connectivity with lateral flow from hillslopes to the channel network. The contributing water from hillslopes pushed water from the flat zones into the drainage canals [*Tetzlaff et al*., 2014], explaining the rise in contribution from both Histosols and Andosols when the flow level increased. Similar connectivity processes were reported by *Ali et al*. [2010], where scenarios that involved high flow and wet antecedent catchment conditions were associated with increased proportions of soil water contribution from slopes in a forested headwater catchment in Canada. From this it can be concluded, as stated by *Jencso et al*. [2009], that the hydrologic connectivity between landscape elements is heterogeneous in time and space.

The increased water contribution from soils near and in the riparian zone when the discharge increased is supported by previous studies in both this region [*Roa-García et al*., 2011; *Mosquera et al*., 2015; *Correa et al*.,

2016] and other ecosystems, such as mountainous landscapes in Scotland [*Tunaley et al*., 2016]. The decreasing contribution of SW as a chemical-rich end-member could be explained by dilution processes when the flow level increases [*Neill et al*., 2011]. With higher water levels, stream water is less imprinted by weathering-derived solutes [*Blumstock et al*., 2015] because of dilution with rainfall and mobile soil water [*Bücker et al*., 2010].

During the different seasons, RF showed low variations in its contribution to runoff. The nearly saturated riparian soils were hydrologically the most important [*Burt*, 2005; *Mosquera et al*., 2016a], even more during the drier season, when 45% of the stream water was estimated to originate from this source. As expected, SW's contributions also played a considerable role during the drier season, while water from the hillslopes barely contributed to the streamflow. The research by *Penna et al*. [2016] also drew this conclusion.

Based on the isotope two-component hydrograph separation, the studied headwater catchment is dominated by preevent water [*Barthold and Woods*, 2015] during wetter and drier seasons. These results are consistent with a previous study in the study area [*Mosquera et al*., 2016a] and the broadly accepted concept that stored water is primarily controlling runoff generation [*McGuire and McDonnell*, 2010; *Klaus and McDonnell*, 2013]. According to the seasonal analysis, the preevent component is slightly reduced during wetter periods, given the higher contribution of water from hillslopes and RF.

Typically for two-component hydrograph separations, small differences between isotopic signatures from the stream and precipitation increased the associated uncertainties to 63%. However, the uncertainty was small throughout the analyzed period (average = 13.5% and Q90 = 27%). Occasionally, the contribution from event water reached high values (>40%). Similarly to previous studies in comparable peat environments, high contributions from event water sporadically occurred during wet periods [*Muñoz-Villers and McDonnell*, 2012; *Tunaley et al*., 2016] or under soil saturation conditions [*McCartney et al*., 1998].

Our analysis of the interannual variations in the water ages of the different contributing water sources with ITTPs provides additional insight into the dynamics, connectivity and mixing processes [*Tetzlaff et al*., 2009; *Soulsby et al*., 2015]. According to the signatures of the soil water ITTPs, the dampening behavior in HS1 was associated with the likely long transit times from the large storage capacity (porosities >80%) in the soils. AN1 with lower storage capacities and rarely saturation conditions did not store the same amount of water, and therefore, the transport velocity (amplitude of the signature) was higher. The effect of young water sources in HS1 on the overall water storage became less pronounced with depth.

Despite being a simplistic approach, our findings from ITTPs are consistent with those from tracer-aid models that were applied to a subannual interpretation of water-age distributions [*Birkel and Soulsby*, 2016; *Tunaley et al*., 2016]. This study revealed older stream water during drier periods and younger stream water during wetter periods, providing a reference for the movement of water through the landscape in different seasons. In North America, and European rivers, young stream water comprises a third of the global river discharge [*Jasechko et al*., 2016], and a higher FYW is expected under wetter conditions, similar to our environment [*Kirchner*, 2016a]. The temporal dynamics of stream ITTPs showed additional event-specific dependencies and nonuniform behavior even during low-flow periods.

During the wettest periods, stream water was influenced by all the Andosol horizons, confirming a high connection with the hillslopes [*Ali et al*., 2010; *van Meerveld et al*., 2015]. Similar results were reported by *Penna et al*. [2015] in a mountain catchment in the Italian pre-Alps. These authors found important contributions from the hillslope's soil water to stream generation under wet conditions. During the drier season, only the deepest Andosol horizon seemed to contribute to Histosols and thus push stored water into streams, which matches previous findings for the Páramo [*Crespo et al*., 2011; *Mosquera et al*., 2016b]. The ITTPs and inferred hydrological connectivity exhibited seasonal variations that were consistent with the research by *Detty and McGuire* [2010]. The younger ITTPs signatures of the superficial horizons during those periods were caused by the low antecedent soil moisture and high porosity of Andosols [*Quichimbo et al*., 2012]. The new water that entered the upper soil horizons rapidly drained towards the bottom without extensive mixing with stored water. In contrast, this mixing occurred during the wetter season and was reflected in an increase in water age (lower ITTP values). During drier periods plotted the older stream water close to the Histosols (Figure 6c), indicating a longer retention time and the overall regulation capacity of the catchment [*Mosquera et al*., 2016a]. Applying ITTPs provided satisfactory results with respect to the interpretation of the hydrologic functioning of the Zhurucay catchment and presented strong potential for

isotope data applications. However, this approach represents a rough approximation of the relative water age, and absolute values should be carefully handled [*Tetzlaff et al*., 2009]. Therefore, we used ITTPs to confirm the results from EMMA and hydrograph separation, increasing the credibility of our conceptual model in Figure 7.

6. Conclusions

Combining End Member Mixing Analysis, hydrograph separation, and water age proxies enabled us to identify and analyze the water flow paths and hydrological processes in a study catchment in the Páramo in southern Ecuador. The relative contribution and timing of different sources from all the methods were in good agreement and strengthened our interpretation of the individual results.

The spatiotemporal dynamics of the dominant water sources and flow paths explained how flow processes change from drier to wetter seasons in the Andean Páramo. A cascade of flow processes is representative for these ecosystems, resulting from the presence of high organic porous soils, a high frequency of precipitation, and the dynamic of the contributing area in the valley bottom, which connects the adjacent hillslopes to the channel network mainly under wet conditions. Rainfall, which is an end-member that represents young water, is a fundamental source to stream water year round. The contribution of spring water, the oldest water, is higher during the drier season. Under wet conditions, water from the Andosols on the hillslopes contributes via the deeper soil horizons towards the Histosols near and in the lower riparian zone. The latter soils represented the dominant contributing water source to streamflow year round, highlighting the importance of the riparian zone. Similarly, the large contributions of preevent water during drier and wetter seasons lead to the same conclusion, which infers that water from such a hydrologically active zone close to the stream plays a relevant role in runoff generation processes. Additionally, evidence of young streamflow during wetter seasons corroborates connectivity between landscape elements, explaining the influence of water from hillslopes.

The uncertainty that underlies some of the applied methods is often discussed (e.g., selection and number of end-members [*Barthold et al*., 2011], estimation of mean transit times, [*Timbe et al*., 2014]). Some studies might suggest focusing more on the uncertainty quantification of individual methods to increase the confidentiality in the obtained results. We used a different approach and applied an ensemble of methods, which enabled us to investigate the structural differences and resulting uncertainty of the various methods and reduce the epistemic uncertainty from our imperfect knowledge of the system. To our knowledge, this study is the first that used the EMMA, hydrograph separation and ITTPs methods to improve the understanding of the hydrological behavior of high mountain tropical catchments. This multimethod approach demonstrated that catchments with perennially humid climates (with drier and wetter periods) and almost stable hydrological conditions can still be characterized by varying interannual source contributions. Understanding of the hydrological functioning can be further improved by analyzing the spatial variability of source contributions within the catchment and by conducting studies to elucidate the contributions over short-time scales, e.g., during events.

Appendix A

Spatial geometry was applied to solve the problem of outliers in the four end-member mixing model, and a scheme is presented in Figure A1a. The stream sample SW plotted outside the tetrahedron that was confined by the four end-members EM1, EM2, EM3, and EM4. Assume that the contribution from EM4 is negative and therefore forced to be zero. SW′ represents the orthogonal projection of SW onto the plane EM1 EM2 EM3.

A plane is a flat, two-dimensional surface in a three-dimensional space that has the equation

$$Ax+By+Cz+D=0$$

$\overrightarrow{EM1\ EM2}$ and $\overrightarrow{EM1\ EM3}$ are vectors from the plane. The cross-product of two vectors results in a vector that is perpendicular to both and therefore normal $\vec{n}$ to the plane that contains them:

$$\overrightarrow{EM1\ EM2} = (EM2_{U1}-EM1_{U1},\ EM2_{U2}-EM1_{U2},\ EM2_{U3}-EM1_{U3})$$

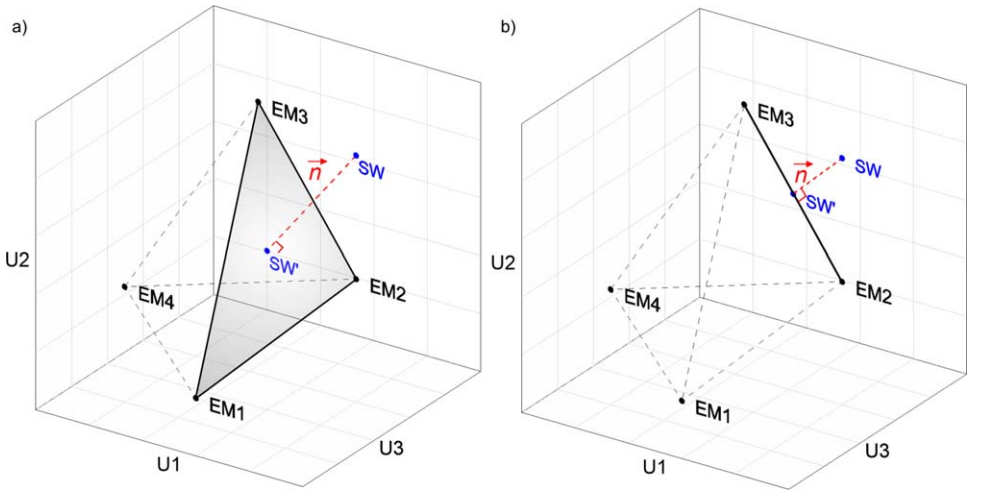

Figure A1. 3-D diagram illustrating how a stream outlier SW is projected in a: (a) plane or (b) line formed by end-members using a spatial geometrical approach.

$$\overrightarrow{EM1\ EM3} = (EM3_{U1} - EM1_{U1},\ EM3_{U2} - EM1_{U2},\ EM3_{U3} - EM1_{U3})$$

$$\overrightarrow{EM1\ EM2}\ X\ \overrightarrow{EM1\ EM3} = (A, B, C) = \vec{n}$$

Consequentially,

$$A = (EM2_{U2} - EM1_{U2})(EM3_{U3} - EM1_{U3}) - (EM3_{U2} - EM1_{U2})(EM2_{U3} - EM1_{U3})$$

$$B = (EM2_{U3} - EM1_{U3})(EM3_{U1} - EM1_{U1}) - (EM3_{U3} - EM1_{U3})(EM2_{U1} - EM1_{U1})$$

$$C = (EM2_{U1} - EM1_{U1})(EM3_{U2} - EM1_{U2}) - (EM3_{U1} - EM1_{U1})(EM2_{U2} - EM1_{U2})$$

$$D = -(A * EM1_{U1} + B * EM1_{U2} + C * EM1_{U3})$$

Consider the line in three-dimensional space through the point SW $(SW_{U1},\ SW_{U2},\ SW_{U3})$ and normal to $Ax + By + Cz + D = 0$. The parametric equations are

$$x = SW_{U1} + A * \lambda$$

$$y = SW_{U2} + B * \lambda$$

$$z = SW_{U3} + C * \lambda$$

The intersection of the plane and normal line that pass through the point SW produces SW′:

$$\lambda = \frac{-(D + A * P_{U1} + B * P_{U2} + C * P_{U3})}{A^2 + B^2 + C^2}$$

The coordinates of the projected point SW′ are

$$SW'_{U1} = SW_{U1} + A * \lambda$$

$$SW'_{U2} = SW_{U2} + B * \lambda$$

$$SW'_{U3} = SW_{U3} + C * \lambda$$

The fractions of the contributions for three end-members (reduction of equations (1)–(4) in the main text) are calculated for SW′ following the equations by *Christophersen et al.* [1990].

If two end-members, such as EM4 and EM1, exhibit negative contributions, both are forced to be zero and the stream sample is projected on the line from EM2 and EM3 (Figure A1b). The fractions of each end-member's contributions are inversely proportional to their distance to SW′. If three end-members exhibit negative contributions, the remaining end-member has a 100% contribution to the stream.

Acknowledgments
This research was funded by the Central Research Office (DIUC) of the Universidad de Cuenca through the projects "Identificación de las relaciones entre las propiedades biofísicas y la respuesta hidrológica en cuencas de páramo húmedo" and "Desarrollo de indicadores eco-hidrológicos funcionales para evaluar la influencia de las laderas y humedales en una cuenca de páramo húmedo," Secretaría de Educación Superior, Ciencia, Tecnología e Innovación (SENESCYT 112–2012), and the German Research Foundation (DFG, BR2238/14–1). The authors thank Matthias Sprenger for his comments on an earlier draft of the manuscript and the staff of Loma Larga Project, Camila Silva, Heike Weller, Irene Cárdenas, Ryan Padrón, Patricio Lazo, and students from the Schools of Civil Engineering and Environmental Engineering of the Universidad de Cuenca for the laboratory work and logistic support during the field campaigns. We are especially grateful for the constructive comments that were provided by the reviewers, which greatly improved the quality of the manuscript. Supporting data are included as six tables in an .xlsx file.

References

Ali, G. A., A. G. Roy, M.-C. Turmel, and F. Courchesne (2010), Source-to-stream connectivity assessment through end-member mixing analysis, *J. Hydrol.*, *392*(3–4), 119–135, doi:10.1016/j.jhydrol.2010.07.049.

Barthold, F. K., and R. A. Woods (2015), Stormflow generation: A meta-analysis of field evidence from small, forested catchments, *Water Resour. Res.*, *51*, 3730–3753, doi:10.1002/2014WR016221.

Barthold, F. K., C. Tyralla, K. Schneider, K. B. Vaché, H. G. Frede, and L. Breuer (2011), How many tracers do we need for end member mixing analysis (EMMA)? A sensitivity analysis, *Water Resour. Res.*, *47*, W08519, doi:10.1029/2011WR010604.

Barthold, F. K., B. L. Turner, H. Elsenbeer, and A. Zimmermann (2017), A hydrochemical approach to quantify the role of return flow in a surface flow-dominated catchment, *Hydrol. Processes*, *31*(5), 1018–1033, doi:10.1002/hyp.11083.

Beck, E., F. Makeschin, F. Haubrich, M. Richter, J. Bendix, and C. Valarezo (2008), The ecosystem (Reserva Biológica San Francisco), in *Gradients in a Tropical Mountain Ecosystem of Ecuador. Ecological Studies*, vol. 198, edited by E. Beck et al., pp. 1–14, Springer, Berlin.

Bergstrom, A., K. Jencso, and B. McGlynn (2016), Spatiotemporal processes that contribute to hydrologic exchange between hillslopes, valley bottoms, and streams: Upland and valley bottom influences on stream water balance, *Water Resour. Res.*, *52*, 4628–4645, doi:10.1002/2015WR017972.

Beven, K. J., and M. J. Kirkby (1979), A physically based, variable contributing area model of basin hydrology [Un modèle à base physique de zone d'appel variable de l'hydrologie du bassin versant], *Hydrol. Sci. Bull.*, *24*(1), 43–69, doi:10.1080/02626667909491834.

Birkel, C., and C. Soulsby (2016), Linking tracers, water age and conceptual models to identify dominant runoff processes in a sparsely monitored humid tropical catchment: Linking tracers, water age and conceptual models in the humid tropics, *Hydrol. Processes*, *30*, 4477–4493, doi:10.1002/hyp.10941.

Birkel, C., J. Geris, M. J. Molina, C. Mendez, R. Arce, J. Dick, D. Tetzlaff, and C. Soulsby (2016), Hydroclimatic controls on non-stationary stream water ages in humid tropical catchments, *J. Hydrol.*, *542*, 231–240, doi:10.1016/j.jhydrol.2016.09.006.

Blumstock, M., D. Tetzlaff, I. A. Malcolm, G. Nuetzmann, and C. Soulsby (2015), Baseflow dynamics: Multi-tracer surveys to assess variable groundwater contributions to montane streams under low flows, *J. Hydrol.*, *527*, 1021–1033, doi:10.1016/j.jhydrol.2015.05.019.

Blumstock, M., D. Tetzlaff, J. J. Dick, G. Nuetzmann, and C. Soulsby (2016), Spatial organization of groundwater dynamics and streamflow response from different hydropedological units in a montane catchment: Groundwater and stream dynamics across different hydropedological units, *Hydrol. Processes*, *30*(21), 3735–3753, doi:10.1002/hyp.10848.

Boll, J., T. S. Steenhuis, and J. S. Selker (1992), Fiberglass wicks for sampling of water and solutes in the Vadose zone, *Soil Sci. Soc. Am. J.*, *56*(3), 701, doi:10.2136/sssaj1992.03615995005600030005x.

Brown, V. A., J. J. McDonnell, D. A. Burns, and C. Kendall (1999), The role of event water, a rapid shallow flow component, and catchment size in summer stormflow, *J. Hydrol.*, *217*(3–4), 171–190, doi:10.1016/S0022-1694(98)00247-9.

Bücker, A., P. Crespo, H.-G. Frede, K. Vaché, and F. Cisneros (2010), Identifying controls on water chemistry of tropical cloud forest catchments: Combining descriptive approaches and multivariate analysis, *Aquat. Geochem.*, *16*(1), 127–149.

Burt, T. P. (2005), A third paradox in catchment hydrology and biogeochemistry: Decoupling in the riparian zone, *Hydrol. Processes*, *19*(10), 2087–2089, doi:10.1002/hyp.5904.

Buttle, J. M. (1994), Isotope hydrograph separations and rapid delivery of pre-event water from drainage basins, *Prog. Phys. Geogr.*, *18*(1), 16–41, doi:10.1177/030913339401800102.

Buytaert, W., G. Wyseure, B. De Bièvre, and J. Deckers (2005), The effect of land-use changes on the hydrological behaviour of Histic Andosols in South Ecuador, *Hydrol. Processes*, *19*(20), 3985–3997, doi:10.1002/hyp.5867.

Buytaert, W., R. Célleri, B. De Bièvre, F. Cisneros, G. Wyseure, J. Deckers, and R. Hofstede (2006), Human impact on the hydrology of the Andean Páramos, *Earth Sci. Rev.*, *79*(1–2), 53–72, doi:10.1016/j.earscirev.2006.06.002.

Buytaert, W., V. Iñiguez, and B. D. Bièvre (2007), The effects of afforestation and cultivation on water yield in the Andean Páramo, *For. Ecol. Manage.*, *251*(1–2), 22–30, doi:10.1016/j.foreco.2007.06.035.

Buytaert, W., R. Celleri, B. De Bièvre, F. Cisneros, G. Wyseure, J. Deckers, and R. Hofstede (2006), Human impact on the hydrology of the Andean Paramos, *Earth Sci. Rev.*, *79*(1-2), 53–72, doi:10.1016/j.earscirev.2006.06.002.

Capell, R., D. Tetzlaff, A. J. Hartley, and C. Soulsby (2012), Linking metrics of hydrological function and transit times to landscape controls in a heterogeneous mesoscale catchment, *Hydrol. Processes*, *26*(3), 405–420, doi:10.1002/hyp.8139.

Célleri, R., and J. Feyen (2009), The hydrology of tropical Andean ecosystems: Importance, knowledge status, and perspectives, *Mt. Res. Dev.*, *29*(4), 350–355, doi:10.1659/mrd.00007.

Chaves, J., C. Neill, S. Germer, S. G. Neto, A. Krusche, and H. Elsenbeer (2008), Land management impacts on runoff sources in small Amazon watersheds, *Hydrol. Processes*, *22*(12), 1766–1775, doi:10.1002/hyp.6803.

Christophersen, N., and R. P. Hooper (1992), Multivariate analysis of stream water chemical data: The use of principal components analysis for end-member mixing problem, *Water Resour. Res.*, *28*(1), 99–107.

Christophersen, N., C. Neal, R. P. Hooper, R. D. Vogt, and S. Andersen (1990), Modelling streamwater chemistry as a mixture of soilwater end-members—A step towards second-generation acidification models, *J. Hydrol.*, *116*(1–4), 307–320.

Coltorti, M., and C. D. Ollier (2000), Geomorphic and tectonic evolution of the Ecuadorian Andes, *Geomorphology*, *32*, 1–19, doi:10.1016/S0169-555X(99)00036-7.

Córdova, M., G. Carrillo-Rojas, P. Crespo, B. Wilcox, and R. Célleri (2015), Evaluation of the Penman-Monteith (FAO 56 PM) method for calculating reference evapotranspiration using limited data: Application to the wet *Páramo* of Southern Ecuador, *Mt. Res. Dev.*, *35*(3), 230–239, doi:10.1659/MRD-JOURNAL-D-14-0024.1.

Correa, A., D. Windhorst, P. Crespo, R. Célleri, J. Feyen, and L. Breuer (2016), Continuous versus event based sampling: How many samples are required for deriving general hydrological understanding on Ecuador's páramo region?: Comparison of continuous versus event based sampling, *Hydrol. Processes*, *30*, 4059–4073, doi:10.1002/hyp.10975.

Crespo, P. J., J. Feyen, W. Buytaert, A. Bücker, L. Breuer, H.-G. Frede, and M. Ramírez (2011), Identifying controls of the rainfall–runoff response of small catchments in the tropical Andes (Ecuador), *J. Hydrol.*, *407*(1–4), 164–174, doi:10.1016/j.jhydrol.2011.07.021.

Delsman, J. R., G. H. P. O. Essink, K. J. Beven, and P. J. Stuyfzand (2013), Uncertainty estimation of end-member mixing using generalized likelihood uncertainty estimation (GLUE), applied in a lowland catchment: Uncertainty estimation of end-member mixing, *Water Resour. Res.*, *49*, 4792–4806, doi:10.1002/wrcr.20341.

Detty, J. M., and K. J. McGuire (2010), Topographic controls on shallow groundwater dynamics: Implications of hydrologic connectivity between hillslopes and riparian zones in a till mantled catchment, *Hydrol. Processes*, *24*(16), 2222–2236, doi:10.1002/hyp.7656.

Engel, M., D. Penna, G. Bertoldi, A. Dell'Agnese, C. Soulsby, and F. Comiti (2016), Identifying run-off contributions during melt-induced run-off events in a glacierized alpine catchment, *Hydrol. Processes*, *30*(3), 343–364, doi:10.1002/hyp.10577.

Favier, V., A. Coudrain, E. Cadier, B. Francou, E. Ayabaca, L. Maisincho, E. Praderio, M. Villacis, and P. Wagnon (2008), Evidence of groundwater flow on Antizana ice-covered volcano, Ecuador [Mise en évidence d'écoulements souterrains sur le volcan englacé Antizana, Equateur], *Hydrol. Sci. J.*, *53*(1), 278–291, doi:10.1623/hysj.53.1.278.

Genereux, D. (1998), Quantifying uncertainty in tracer-based hydrograph separations, *Water Resour. Res.*, *34*(4), 915–919, doi:10.1029/98WR00010.

Hooper, R. P. (2001), Applying the scientific method to small catchment studies: A review of the Panola Mountain experience, *Hydrol. Processes*, *15*(10), 2039–2050, doi:10.1002/hyp.255.

Hooper, R. P. (2003), Diagnostic tools for mixing models of stream water chemistry, *Water Resour. Res.*, *39*(3), 1055, doi:10.1029/2002WR001528.

Hugenschmidt, C., J. Ingwersen, W. Sangchan, Y. Sukvanachaikul, A. Duffner, S. Uhlenbrook, and T. Streck (2014), A three-component hydrograph separation based on geochemical tracers in a tropical mountainous headwater catchment in northern Thailand, *Hydrol. Earth Syst. Sci.*, *18*(2), 525–537, doi:10.5194/hess-18-525-2014.

Inamdar, S., G. Dhillon, S. Singh, S. Dutta, D. Levia, D. Scott, M. Mitchell, J. Van Stan, and P. McHale (2013), Temporal variation in end-member chemistry and its influence on runoff mixing patterns in a forested, Piedmont catchment, *Water Resour. Res.*, *49*, 1828–1844, doi:10.1002/wrcr.20158.

Iwasaki, K., M. Katsuyama, and M. Tani (2015), Contributions of bedrock groundwater to the upscaling of storm-runoff generation processes in weathered granitic headwater catchments, *Hydrol. Processes*, *29*(6), 1535–1548, doi:10.1002/hyp.10279.

James, A. L., and N. T. Roulet (2006), Investigating the applicability of end-member mixing analysis (EMMA) across scale: A study of eight small, nested catchments in a temperate forested watershed, *Water Resour. Res.*, *42*, 1–17, doi:10.1029/2005WR004419.

Jasechko, S., J. W. Kirchner, J. M. Welker, and J. J. McDonnell (2016), Substantial proportion of global streamflow less than three months old, *Nat. Geosci.*, *9*(2), 126–129, doi:10.1038/ngeo2636.

Jencso, K. G., B. L. McGlynn, M. N. Gooseff, S. M. Wondzell, K. E. Bencala, and L. A. Marshall (2009), Hydrologic connectivity between landscapes and streams: Transferring reach- and plot-scale understanding to the catchment scale, *Water Resour. Res.*, *45*, W04428, doi:10.1029/2008WR007225.

Josse, C., F. Cuesta, G. Navarro, V. Barrena, E. Cabrera, E. Chacón-Moreno, W. Ferreira, M. Perlavo, J. Saito, and A. Tovar (2009), Ecosistemas de los Andes del Norte y Centro. Bolivia, Colombia, Ecuador, Perú y Venezuela. Secretaría General de la Comunidad Andina, Programa Regional ECOBONA-Intercooperation, CONDESAN-Proyecto Páramo Andino, Programa BioAndes, EcoCiencia, NatureServe, IAvH, LTA-UNALM, ICAE-ULA, CDC-UNALM, RUMBOL SRL. Lima.

Katsuyama, M., N. Ohte, and S. Kobashi (2001), A three-component end-member analysis of streamwater hydrochemistry in a small Japanese forested headwater catchment, *Hydrol. Processes*, *15*(2), 249–260.

Kirchner, J. W. (2016a), Aggregation in environmental systems—Part 1: Seasonal tracer cycles quantify young water fractions, but not mean transit times, in spatially heterogeneous catchments, *Hydrol. Earth Syst. Sci.*, *20*(1), 279–297, doi:10.5194/hess-20-279-2016.

Kirchner, J. W. (2016b), Aggregation in environmental systems—Part 2: Catchment mean transit times and young water fractions under hydrologic nonstationarity, *Hydrol. Earth Syst. Sci.*, *20*(1), 299–328, doi:10.5194/hess-20-299-2016.

Klaus, J., and J. J. McDonnell (2013), Hydrograph separation using stable isotopes: Review and evaluation, *J. Hydrol.*, *505*, 47–64, doi:10.1016/j.jhydrol.2013.09.006.

Ladouche, B., A. Probst, D. Viville, S. Idir, D. Baqué, M. Loubet, J.-L. Probst, and T. Bariac (2001), Hydrograph separation using isotopic, chemical and hydrological approaches (Strengbach catchment, France), *J. Hydrol.*, *242*(3–4), 255–274, doi:10.1016/S0022-1694(00)00391-7.

Lana-Renault, N., D. Regüés, P. Serrano, and J. Latron (2014), Spatial and temporal variability of groundwater dynamics in a sub-Mediterranean mountain catchment, *Hydrol. Processes*, *28*(8), 3288–3299, doi:10.1002/hyp.9892.

Lee, E. S., and N. C. Krothe (2001), A four-component mixing model for water in a karst terrain in south-central Indiana, USA. Using solute concentration and stable isotopes as tracers, *Chem. Geol.*, *179*(1–4), 129–143, doi:10.1016/S0009-2541(01)00319-9.

Liu, F., M. W. Williams, and N. Caine (2004), Source waters and flow paths in an alpine catchment, Colorado Front Range, United States, *Water Resour. Res.*, *40*, W09401, doi:10.1029/2004WR003076.

McCartney, M. P., C. Neal, and M. Neal (1998), Use of deuterium to understand runoff generation in a headwater catchment containing a dambo, *Hydrol. Earth Syst. Sci.*, *2*(1), 65–76, doi:10.5194/hess-2-65-1998.

McDonnell, J. J. (2003), Where does water go when it rains? Moving beyond the variable source area concept of rainfall-runoff response, *Hydrol. Processes*, *17*(9), 1869–1875, doi:10.1002/hyp.5132.

McGlynn, B. L., and J. J. McDonnell (2003), Quantifying the relative contributions of riparian and hillslope zones to catchment runoff, *Water Resour. Res.*, *39*(11), 1310, doi:10.1029/2003WR002091.

McGuire, K. J., and J. J. McDonnell (2006), A review and evaluation of catchment transit time modeling, *J. Hydrol.*, *330*(3–4), 543–563, doi:10.1016/j.jhydrol.2006.04.020.

McGuire, K. J., and J. J. McDonnell (2010), Hydrological connectivity of hillslopes and streams: Characteristic time scales and nonlinearities: Hydrological connectivity of hillslopes and streams, *Water Resour. Res.*, *46*, W10543, doi:10.1029/2010WR009341.

Mosquera, G. M., P. X. Lazo, R. Célleri, B. P. Wilcox, and P. Crespo (2015), Runoff from tropical alpine grasslands increases with areal extent of wetlands, *Catena*, *125*, 120–128, doi:10.1016/j.catena.2014.10.010.

Mosquera, G. M., R. Célleri, P. X. Lazo, K. B. Vaché, S. S. Perakis, and P. Crespo (2016a), Combined use of isotopic and hydrometric data to conceptualize ecohydrological processes in a high-elevation tropical ecosystem, *Hydrol. Processes*, *30*, 2930–2947, doi:10.1002/hyp.10927.

Mosquera, G. M., C. Segura, K. B. Vaché, D. Windhorst, L. Breuer, and P. Crespo (2016b), Insights into the water mean transit time in a high-elevation tropical ecosystem, *Hydrol. Earth Syst. Sci.*, *20*(7), 2987–3004, doi:10.5194/hess-20-2987-2016.

Muñoz-Villers, L. E., and J. J. McDonnell (2012), Runoff generation in a steep, tropical montane cloud forest catchment on permeable volcanic substrate: Storm runoff in a montane forest, *Water Resour. Res.*, *48*, W09528, doi:10.1029/2011WR011316.

Neill, C., et al. (2011), Runoff sources and land cover change in the Amazon: An end-member mixing analysis from small watersheds, *Biogeochemistry*, *105*(1–3), 7, doi:10.1007/s10533-011-9597-8.

Ochoa-Tocachi, B. F., et al. (2016), Impacts of land use on the hydrological response of tropical Andean catchments, *Hydrol. Processes*, *30*, 4074–4089, doi:10.1002/hyp.10980.

Padrón, R. S., B. P. Wilcox, P. Crespo, and R. Célleri (2015), Rainfall in the Andean Páramo: New insights from high-resolution monitoring in Southern Ecuador, *J. Hydrometeorol.*, *16*(3), 985–996, doi:10.1175/JHM-D-14-0135.1.

Penna, D., H. J. van Meerveld, O. Oliviero, G. Zuecco, R. S. Assendelft, G. Dalla Fontana, and M. Borga (2015), Seasonal changes in runoff generation in a small forested mountain catchment, *Hydrol. Processes*, *29*(8), 2027–2042, doi:10.1002/hyp.10347.

Penna, D., H. J. van Meerveld, G. Zuecco, G. Dalla Fontana, and M. Borga (2016), Hydrological response of an Alpine catchment to rainfall and snowmelt events, *J. Hydrol.*, *537*, 382–397, doi:10.1016/j.jhydrol.2016.03.040.

Picarro (2010), ChemCorrect™—Solving the problem of chemical contaminants in H_2O stable isotope research, white paper, pp. 2–4, Picarro Inc. Sunnyvale, Calif. [Available at http://www.picarro.com/assets/docs/Picarro_-_ChemCorrect_White_Paper.pdf.]

Pratt, W. T., J. F. Figueroa, and B. C. Flores (1997), Geology of the Cordillera Occidental of Ecuador between 3*00′ and 4*00′S: British Geological Survey Open File Rep., WC/97/28. 98 pp.

Quichimbo, P., G. Tenorio, P. Borja, I. Cárdenas, P. Crespo, and R. Célleri (2012), Efectos sobre las propiedades físicas y químicas de los suelos por el cambio de la cobertura vegetal y uso del suelo: Páramo de Quimsacocha al sur del Ecuador, *Suelos Ecuat.*, *42*(2), 138–153.

Rinderer, M., H. J. van Meerveld, and J. Seibert (2014), Topographic controls on shallow groundwater levels in a steep, prealpine catchment: When are the TWI assumptions valid?, *Water Resour. Res.*, *50*, 6067–6080, doi:10.1002/2013WR015009.

Rinderer, M., I. van Meerveld, M. Stähli, and J. Seibert (2016), Is groundwater response timing in a pre-alpine catchment controlled more by topography or by rainfall?, *Hydrol. Processes*, *30*(7), 1036–1051, doi:10.1002/hyp.10634.

Roa-García, M. C., S. Brown, H. Schreier, and L. M. Lavkulich (2011), The role of land use and soils in regulating water flow in small headwater catchments of the Andes, *Water Resour. Res.*, *47*, W05510, doi:10.1029/2010WR009582.

Seeger, S., and M. Weiler (2014), Reevaluation of transit time distributions, mean transit times and their relation to catchment topography, *Hydrol. Earth Syst. Sci.*, *18*(12), 4751–4771, doi:10.5194/hess-18-4751-2014.

Shaw, G. D., M. H. Conklin, G. J. Nimz, and F. Liu (2014), Groundwater and surface water flow to the Merced River, Yosemite Valley, California: ^{36}Cl and Cl^- evidence, *Water Resour. Res.*, *50*, 1943–1959, doi:10.1002/2013WR014222.

Soulsby, C., D. Tetzlaff, P. Rodgers, S. Dunn, and S. Waldron (2006), Runoff processes, stream water residence times and controlling landscape characteristics in a mesoscale catchment: An initial evaluation, *J. Hydrol.*, *325*(1–4), 197–221, doi:10.1016/j.jhydrol.2005.10.024.

Soulsby, C., C. Birkel, J. Geris, J. Dick, C. Tunaley, and D. Tetzlaff (2015), Stream water age distributions controlled by storage dynamics and nonlinear hydrologic connectivity: Modeling with high-resolution isotope data, *Water Resour. Res.*, *51*, 7759–7776, doi:10.1002/2015WR017888.

Tetzlaff, D., J. Seibert, K. J. Mcguire, D. A. Burns, S. M. Dunn, and C. Soulsby (2009), How does landscape structure influence catchment transit time across geomorphologic provinces?, *Hydrol. Processes*, *23*, 945–953, doi:10.1002/hyp.7240.

Tetzlaff, D., C. Birkel, J. Dick, J. Geris, and C. Soulsby (2014), Storage dynamics in hydropedological units control hillslope connectivity, runoff generation, and the evolution of catchment transit time distributions, *Water Resour. Res.*, *50*, 969–985, doi:10.1002/2013WR014147.

Timbe, E., D. Windhorst, P. Crespo, H.-G. Frede, J. Feyen, and L. Breuer (2014), Understanding uncertainties when inferring mean transit times of water trough tracer-based lumped-parameter models in Andean tropical montane cloud forest catchments, *Hydrol. Earth Syst. Sci.*, *18*, 1503–1523.

Tunaley, C., D. Tetzlaff, J. Lessels, and C. Soulsby (2016), Linking high-frequency DOC dynamics to the age of connected water sources: Linking doc to flow paths and water ages, *Water Resour. Res.*, *52*, 5232–5247, doi:10.1002/2015WR018419.

van Meerveld, H. J., J. Seibert, and N. E. Peters (2015), Hillslope–riparian-stream connectivity and flow directions at the Panola Mountain Research Watershed, *Hydrol. Process.*, *29*(16), 3556–3574, doi:10.1002/hyp.10508.

von Freyberg, J., D. Radny, H. E. Gall, and M. Schirmer (2014), Implications of hydrologic connectivity between hillslopes and riparian zones on streamflow composition, *J. Contam. Hydrol.*, *169*, 62–74, doi:10.1016/j.jconhyd.2014.07.005.

Windhorst, D., T. Waltz, E. Timbe, H.-G. Frede, and L. Breuer (2013), Impact of elevation and weather patterns on the isotopic composition of precipitation in a tropical montane rainforest, *Hydrol. Earth Syst. Sci.*, *17*(1), 409–419, doi:10.5194/hess-17-409-2013.